

First Constraint on Coherent Elastic Neutrino-Nucleus Scattering in Argon

D. Akimov,^{1,2} J.B. Albert,³ P. An,^{4,5} C. Awe,^{4,5} P.S. Barbeau,^{4,5} B. Becker,⁶ V. Belov,^{1,2} M.A. Blackston,⁷ A. Bolozdynya,² B. Cabrera-Palmer,⁸ M. Cervantes,⁴ J.I. Collar,^{9,10} R.L. Cooper,^{11,12} J. Daughhetee,⁶ M. del Valle Coello,³ J.A. Detwiler,¹³ M. D’Onofrio,³ Y. Efremenko,^{6,7} E.M. Erkela,¹³ S.R. Elliott,¹² L. Fabris,⁷ M. Febraro,⁷ W. Fox,³ A. Galindo-Uribarri,^{6,7} M.P. Green,^{5,7,14} K.S. Hansen,¹³ M.R. Heath,³ S. Hedges,^{4,5} T. Johnson,^{4,5} M. Kaemingk,¹¹ L.J. Kaufman,³ A. Khromov,² A. Kononov,^{1,2} E. Kozlova,^{1,2} A. Kumpan,² L. Li,^{4,5} J.T. Librande,¹³ J.M. Link,¹⁵ J. Liu,¹⁶ K. Mann,^{5,7} D.M. Markoff,^{5,17} H. Moreno,¹¹ P.E. Mueller,⁷ J. Newby,⁷ D.S. Parno,¹⁸ S. Penttila,⁷ D. Pershey,⁴ D. Radford,⁷ R. Rapp,¹⁸ H. Ray,¹⁹ J. Raybern,⁴ O. Razuvaeva,^{1,2} D. Reyna,⁸ G.C. Rich,⁹ D. Rudik,^{1,2} J. Runge,^{4,5} D.J. Salvat,^{3,13} K. Scholberg,⁴ A. Shakirov,² G. Simakov,^{1,2} G. Sinev,⁴ W.M. Snow,³ V. Sosnovtsev,² B. Suh,³ R. Tayloe,³ K. Tellez-Giron-Flores,¹⁵ R.T. Thornton,^{3,12} I. Tolstukhin,³ J. Vanderwerp,³ R.L. Varner,⁷ C.J. Virtue,²⁰ G. Visser,³ C. Wiseman,¹³ T. Wongjirad,²¹ J. Yang,²¹ Y.-R. Yen,¹⁸ J. Yoo,²² C.-H. Yu,⁷ and J. Zettlemoyer^{3,7}

¹*Institute for Theoretical and Experimental Physics named by A.I. Alikhanov of National Research Centre “Kurchatov Institute”, Moscow, 117218, Russian Federation*

²*National Research Nuclear University MEPhI (Moscow Engineering Physics Institute), Moscow, 115409, Russian Federation*

³*Department of Physics, Indiana University, Bloomington, IN, 47405, USA*

⁴*Department of Physics, Duke University, Durham, NC 27708, USA*

⁵*Triangle Universities Nuclear Laboratory, Durham, NC 27708, USA*

⁶*Department of Physics and Astronomy, University of Tennessee, Knoxville, TN 37996, USA*

⁷*Oak Ridge National Laboratory, Oak Ridge, TN 37831, USA*

⁸*Sandia National Laboratories, Livermore, CA 94550, USA*

⁹*Enrico Fermi Institute and Kavli Institute for Cosmological Physics, University of Chicago, Chicago, IL 60637, USA*

¹⁰*Department of Physics, University of Chicago, Chicago, IL 60637, USA*

¹¹*Department of Physics, New Mexico State University, Las Cruces, NM 88003, USA*

¹²*Los Alamos National Laboratory, Los Alamos, NM, USA, 87545, USA*

¹³*Center for Experimental Nuclear Physics and Astrophysics & Department of Physics, University of Washington, Seattle, WA 98195, USA*

¹⁴*Department of Physics, North Carolina State University, Raleigh, NC 27695, USA*

¹⁵*Center for Neutrino Physics, Virginia Tech, Blacksburg, VA 24061, USA*

¹⁶*Physics Department, University of South Dakota, Vermillion, SD 57069, USA*

¹⁷*Department of Mathematics and Physics, North Carolina Central University, Durham, NC 27707, USA*

¹⁸*Department of Physics, Carnegie Mellon University, Pittsburgh, PA 15213, USA*

¹⁹*Department of Physics, University of Florida, Gainesville, FL 32611, USA*

²⁰*Department of Physics, Laurentian University, Sudbury, Ontario P3E 2C6, Canada*

²¹*Department of Physics and Astronomy, Tufts University, Medford, MA 02155, USA*

²²*Department of Physics at Korea Advanced Institute of Science and Technology (KAIST) and Center for Axion and Precision Physics Research (CAPP) at Institute for Basic Science (IBS), Daejeon, 34141, Republic of Korea*

(Dated: September 2019)

Coherent elastic neutrino-nucleus scattering (CEvNS) is the dominant neutrino scattering channel for neutrinos of energy $E_\nu < 100$ MeV. We report a limit for this process using data collected in an engineering run of the 29 kg CENNS-10 liquid argon detector located 27.5 m from the Oak Ridge National Laboratory Spallation Neutron Source (SNS) Hg target with 4.2×10^{22} protons on target. The dataset yielded < 7.4 observed CEvNS events implying a cross section for the process, averaged over the SNS pion decay-at-rest flux, of $< 3.4 \times 10^{-39}$ cm², a limit within twice the Standard Model prediction. This is the first limit on CEvNS from an argon nucleus and confirms the earlier CsI[Na] non-standard neutrino interaction constraints from the collaboration. This run demonstrated the feasibility of the ongoing experimental effort to detect CEvNS with liquid argon.

INTRODUCTION

Coherent elastic neutrino-nucleus scattering (CEvNS), predicted in 1974 as a consequence of the neutral weak current [1, 2], is the dominant neutrino interaction for neutrinos of energy $E_\nu < 100$ MeV. It has a characteristic dependence on the square of the number of neutrons (N^2) reflecting the coherent sum of the weak charge carried by the neutrons, and is sensitive to nuclear physics

effects [3–8] through the nuclear form factor, ($F(Q^2)$), as seen in the differential cross section for a spin-zero nucleus [3]:

$$\frac{d\sigma}{dT} = \frac{G_F^2 M}{2\pi} \left[2 - \frac{2T}{E_\nu} + \left(\frac{T}{E_\nu} \right)^2 - \frac{MT}{E_\nu^2} \right] \frac{Q_W^2}{4} F^2(Q^2) \quad (1)$$

where T is the recoil energy, M is the mass of the nucleus, and $Q_W = N - Z (1 - 4 \sin^2 \theta_W)$ is the weak charge

with weak mixing angle θ_W . CEvNS is also sensitive to physics beyond the Standard Model (SM) [9–14]. In particular, the ability of a CEvNS measurement to constrain so-called “Non-Standard Interactions” (NSI) is critical as their presence can confound the mass ordering determination by long-baseline neutrino experiments such as DUNE [15–17].

CEvNS has eluded detection until recently due to the challenging technical requirements: $\mathcal{O}(10\text{ keV})$ nuclear recoil energy thresholds, intense sources/large target masses, and low backgrounds. The COHERENT collaboration has recently overcome these challenges with state-of-the-art detector technology combined with the intense, pulsed, stopped-pion neutrino source available at the Spallation Neutron Source (SNS) at Oak Ridge National Laboratory (ORNL), using a CsI[Na] crystal to achieve the first measurement of CEvNS [18].

The next step for this program is a demonstration of the N^2 cross section dependence via observation of the process in other nuclei. To that end, the 29 kg liquid argon detector CENNS-10 was commissioned as part of the COHERENT experiment. We report here results from CENNS-10 as configured for an initial engineering run to establish the scintillation response, light yield, and energy calibration of the detector, as well as characterize the expected backgrounds. The results reported here informed a detector upgrade for a longer-term CEvNS search with improved light yield and background reduction.

EXPERIMENT

The ORNL SNS produces neutrons via a 1.4 MW, 1 GeV proton beam pulsed at 60 Hz on a liquid-Hg target (with a typical proton beam trace having a FWHM = 360 ns). This beam also produces copious charged pions leading to a large neutrino flux via π^+ decay-at-rest (DAR). While the total integrated beam power may be known to $<1\%$, the total neutrino flux is only known to 10% due to systematic uncertainties in the pion production rate at the SNS, predicted to be $0.09\pi^+$ for each proton-on-target (POT) at the beam energy for this run period [18]. These π^+ produce a prompt ($\tau = 26\text{ ns}$) 29.8 MeV ν_μ along with a μ^+ which then decays, yielding a delayed ($\tau = 2.2\text{ }\mu\text{s}$) 3-body spectrum of $\bar{\nu}_\mu$, ν_e , and e^+ with an endpoint of 53 MeV. The majority of π^- and μ^- capture on nuclei within the target yielding a very pure π^+ DAR neutrino flux. The pulsed nature of the SNS beam allows for a large reduction in beam-unrelated backgrounds for neutrino experiments.

After a campaign of background measurements in the SNS experimental hall, a low-background area in a basement corridor was identified as a suitable area in which to measure CEvNS. This corridor (“Neutrino Alley”), is shielded by $\gtrsim 20\text{ m}$ of concrete and gravel from the SNS

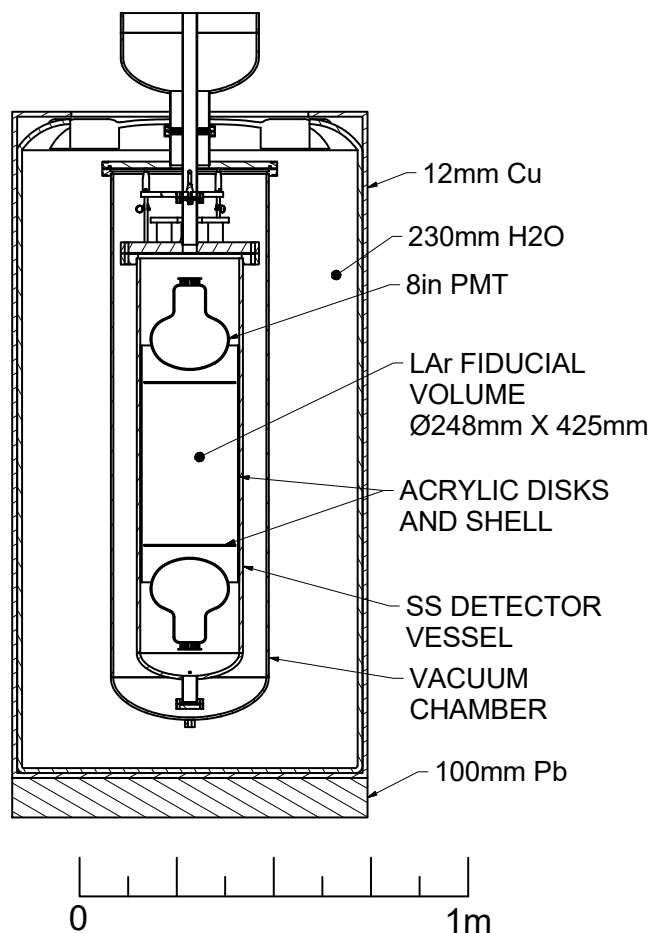


FIG. 1. CENNS-10 liquid argon detector and shielding as configured for this engineering run.

target assembly and by 8 meter water equivalent overburden. This provides a space with a low total background rate and, in particular, a sufficiently low beam-related-neutron rate for a measurement of CEvNS.

In late 2016 the CENNS-10 detector, a single-phase liquid-argon (LAr) scintillation detector (Fig. 1) [19], was installed in Neutrino Alley 27.5 m from the SNS target. CENNS-10 was initially built at Fermilab for a prototype experiment [20] to run near the Fermilab Booster neutrino source. It contains a total LAr mass of 79.5 kg.

For this engineering run, a 29 kg active detector mass was defined by a surrounding acrylic cylindrical shell coated with 0.2 mg cm^{-2} TPB (tetraphenyl-butadiene) to wavelength-shift the 128 nm argon scintillation light to a distribution with $\lambda_{peak} \approx 400\text{ nm}$ [21–24]. This visible light was viewed with two 8” diameter Hamamatsu R5912-02MOD photomultiplier tubes (PMTs) read out with a CAEN V1720 digitizer. The LAr, cooled and liquified with a 90 W Cryomech PT-90 cold head, was contained in a stainless-steel detector vessel within a vacuum cryostat. As seen in Fig. 1, the cryostat was suspended in a cylindrical water tank which was further contained

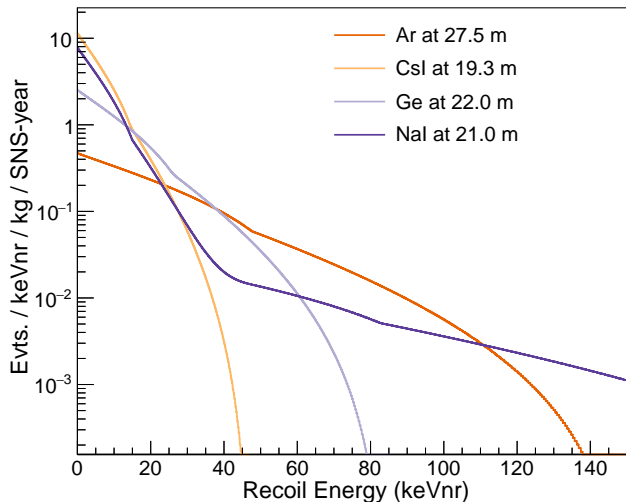


FIG. 2. Nuclear recoil kinetic energy distribution from CEvNS for the SNS neutrino spectrum for currently-deployed and planned COHERENT detectors at their respective detector locations in Neutrino Alley.

within an external copper layer sitting on a layer of lead. The water layer reduces the beam-related neutron backgrounds, the lead is designed to reduce the flux from environmental γ backgrounds, and the copper is added to shield from x-rays produced from ^{210}Pb β decays in the lead.

This engineering run coincided with three months of SNS neutron production corresponding to a total integrated beam power of 1.8 GWhr (4.2×10^{22} POT) at an average energy of 973 MeV. A CEvNS search was performed with 1.5 GWhr of beam following the completion of the full-shielding (water and copper) installation. Data were read from the digitizer in 33 μs windows centered around the 60 Hz beam spills. In addition to these “beam” triggers, identical windows (“strobe” triggers) were read asynchronously with the beam spills to precisely characterize beam-unrelated events.

LAr is a natural choice as a medium to detect CEvNS. It provides a light nucleus in contrast to CsI to test the N^2 dependence of the CEvNS cross section. Argon has been widely used for both dark matter WIMP searches [25, 26] and for neutrino detection [27], and has therefore been well-characterized in the literature. It has a high light yield, 40 photons/keVee [28] (electron equivalent energy deposition), providing a sufficiently low threshold for CEvNS detection, and the quenched response to nuclear recoils has been well-characterized [29–32] allowing for well-understood CEvNS predictions. LAr scintillates on two significantly different time scales ($\tau_{\text{singlet}} \approx 6$ ns, $\tau_{\text{triplet}} \approx 1600$ ns) [33] providing powerful pulse-shape discrimination (PSD) capabilities to separate nuclear from electronic recoils (NR and ER respectively) [34–36]. Both the light output and PSD capabili-

ties depend on the LAr purity.

As seen in Fig. 2, the CEvNS process in LAr with the SNS neutrino source produces nuclear recoils up to ~ 100 keVnr (nuclear recoil). Due to the low-energy recoil signal, and the low event rates, the expected backgrounds need to be well characterized. In Neutrino Alley, CENNS-10 is sensitive to both beam-related and beam-unrelated backgrounds. These beam-unrelated backgrounds typically cause electronic recoils and are dominated by a high flux of 511 keV gamma rays from a pipe running through Neutrino Alley carrying radioactive gas from the SNS target system. The PSD capabilities of LAr are used to reject most of these events; the rate of those remaining in the sample is measured via the strobe windows. In a strict sense, these 511 keV gamma rays are beam-related and their rates change with the time history of accelerator operations. However, as the rate of change is small compared to the beam pulse rate, they are characterized as beam-unrelated. External beam-unrelated backgrounds have largely been mitigated in a subsequent run of CENNS-10 with the installation of additional Pb shielding, making ^{39}Ar the dominant beam-unrelated background. The ^{39}Ar isotope is cosmogenically produced and is inherent in atmospheric sources of Ar. COHERENT is considering the use of underground argon depleted in ^{39}Ar [37–39] for future LAr measurements.

A more challenging background for a CEvNS analysis is caused by beam-related neutrons (BRNs) produced in the SNS target. BRNs arrive in-time with the SNS beam pulse and elastically scatter, generating nuclear recoils and mimicking the CEvNS signal. To characterize the BRN flux in energy and time, it was measured by the SciBath detector [20, 40] at the CENNS-10 location in late 2015. This measurement indicated that the BRN flux in time with the beam pulse is substantial compared to the prompt CEvNS signal while the delayed BRN flux is negligible, thus providing a suitable time window in which to search for CEvNS [41].

ANALYSIS

The analysis of this dataset proceeded as follows: First a suite of radioactive γ and neutron sources were used to calibrate the detector energy and PSD response and the detector simulation was tuned to match these data. Then beam-unrelated backgrounds were measured with strobe triggers, the beam-related background from BRNs was predicted with simulation based on the previous SciBath measurement, and the CEvNS signal was predicted from the SM cross section. Energy, PSD, and time cuts were then optimized with those estimates to maximize beam-related signal significance. With those cuts, a reduced neutron-shielding dataset was used to adjust the BRN prediction for the full shielded configuration. Fi-

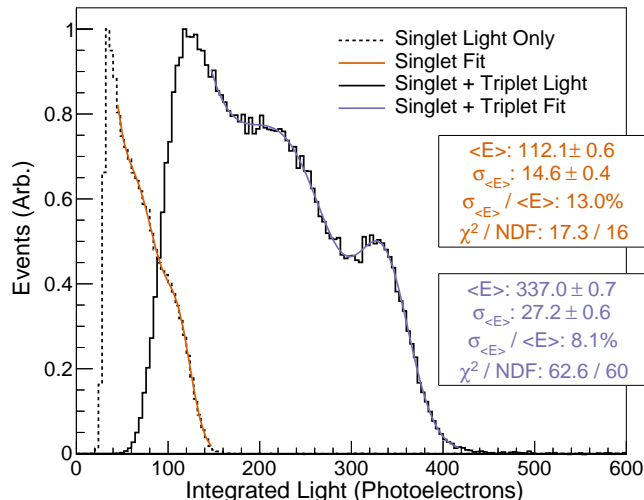


FIG. 3. Reconstructed energy spectrum with a ^{137}Cs source. The singlet pulse fitting allows for the singlet light to be summed separately.

nally, cuts were optimized and fixed for both a ‘counting experiment’ and a likelihood fit before analyzing the full shielded beam-on dataset.

The individual, digitized PMT waveforms are analyzed for every trigger in the data stream and saturated waveforms are removed from the dataset. A baseline is determined from the average ADC value in the first 1 μs of each remaining waveform. This baseline is then used to identify PMT pulses on each channel above a 20 ADC (~ 2 photoelectron) threshold. Events are identified when there are coincident PMT signals above this threshold to avoid triggering on single photoelectron-level pulses from PMT dark rate. A requirement that the maximum ADC value occur within the first 90 ns of the event minimizes the effects from event pileup. A local baseline is calculated immediately before each pulse and a least-squares parabola fit is performed to the pulse peak for an accurate singlet pulse-height measurement. The results from the parabola fit are used to fit a single photoelectron (SPE) template shape to the singlet peak and the residual between the SPE template and the data is taken. Finally, the integral of the residual waveform is taken as a measure of the amount of triplet light in the event. A pulse shape parameter (F_{prompt} defined as the ratio of singlet to total light) can then be calculated to separate ER background events from the NR CEvNS signal.

Weekly calibration datasets with a ^{137}Cs source were used to measure the detector light output as well as track any changes over the course of this run. The detected photon yield was 0.6 PE/keVee as determined from the observed 662 keV photopeak from the summed singlet and triplet light in the ^{137}Cs spectrum (Fig. 3). It should be noted that the light yield was increased by a factor of 8 in a subsequent upgrade of this detector. With the use

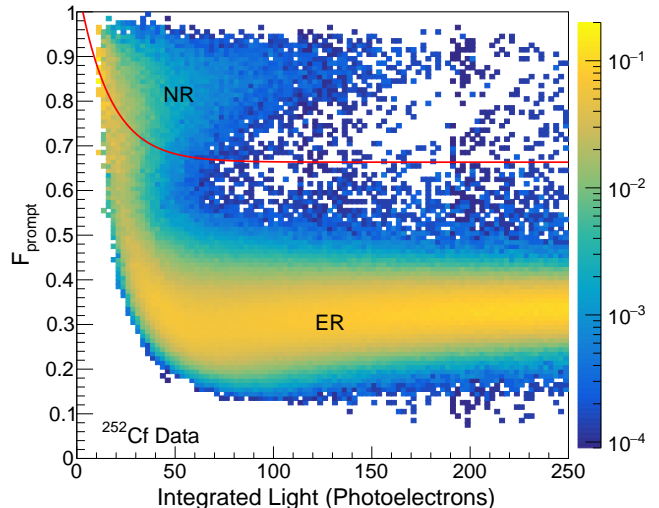


FIG. 4. Distribution of the F_{prompt} parameter as a function of detected light in ^{252}Cf calibration data with decays to both neutrons and γ s. The overlaid red curve is a PSD cut optimized for the cuts-based counting experiment analysis discussed in the text.

of the ^{137}Cs datasets, the triplet lifetime in CENNS-10 was measured to be $\mathcal{O}(1.2 \mu\text{s})$, consistent with an impurity level on the order of $\mathcal{O}(1 \text{ ppm})$ [42], adequate for a scintillation-only detector.

Monthly datasets collected with a ^{252}Cf fission source were used to characterize the response of CENNS-10 to NR events. The separation of NR and ER events in the ^{252}Cf dataset is shown in Fig. 4 where the band at low F_{prompt} is identified as due to ER events and that at high F_{prompt} is identified as NR events due to the fission neutrons. The observed F_{prompt} is consistent with the expected singlet:triplet ratios of ER and NR events [33].

These calibration datasets enabled the tuning of the CENNS-10 Geant4-based [43] Monte Carlo (MC) simulation optical properties for both ER and NR events. These detector simulations were used to evaluate the efficiency for low-energy NR events to be detected and to form predictions of the expected BRN and CEvNS event rates in CENNS-10. An energy-independent fit over the energy range of interest to the global LAr data on nuclear recoil scintillation quenching [29–32] provided a quenching factor (0.289 ± 0.035) for NR vs ER response in CENNS-10. With these waveform analysis and calibration procedures, each detector event can be identified as an ER or NR candidate and be assigned a corresponding energy with units of keVee or keVnr.

Initial BRN predictions using a simulation based on the 2015 SciBath measurement were compared to a dedicated two-week minimal-neutron-shielding dataset. From this comparison, the predicted BRN rate was found to be 20% lower than the observed rate. This factor was used to adjust the expected neutron rates for the primary

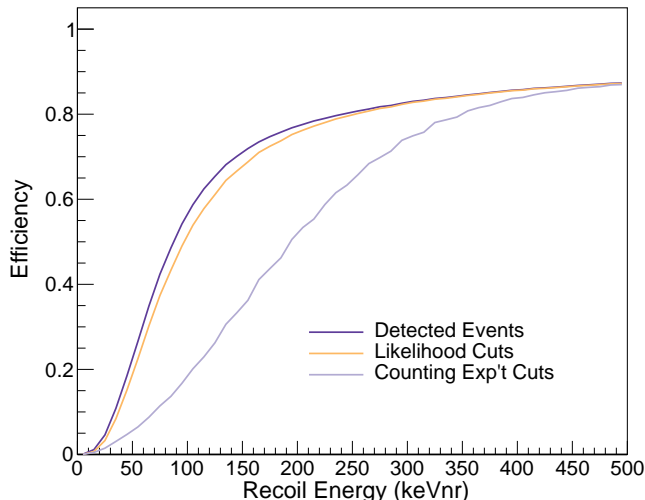


FIG. 5. Estimated efficiency for acceptance of nuclear recoil events in CENNS-10 as function of nuclear recoil energy. “Detected Events” are those that pass the 2PE coincidence required for event building. The likelihood and counting experiment cuts reflect the change in efficiency due to analysis cuts discussed in the text.

CEvNS dataset. However, the BRN normalization was allowed to float in the final analysis. CEvNS predictions were based on the convolution of the pion decay-at-rest neutrino flux and SNS pion-production rate [18] with the Standard Model-predicted CEvNS cross section. Beam-unrelated backgrounds were measured *in situ* with strobe triggers.

Both a cuts-based (“counting experiment”) analysis and a likelihood fit in energy, time, and F_{prompt} space were performed on the full-shielded CEvNS dataset. In the cuts-based analysis, to form a CEvNS sample, a figure-of-merit $\mathcal{F} \equiv N_{sig}/\sigma_{sig}$ was optimized to set a 0–30 keVee reconstructed energy range, a delayed $1.4 < t_{Trig} < 4.4 \mu\text{s}$ time window (where t_{Trig} is measured relative to a timing signal provided by the SNS close to the onset of POT), and an energy-dependent PSD selection seen in Fig. 4. For this analysis, it was assumed that the BRNs observed in Neutrino Alley are produced by fast neutrons from the target scattering in the shielding near the detector and that the neutrinos should arrive roughly 30 ns before the fast neutron peak determined from the BRN measurements. The results reported here are not sensitive to this assumption. A BRN-enhanced sample was selected with an expanded energy range (0–700 keVee) in both the prompt ($0.4 < t_{Trig} < 1.4 \mu\text{s}$) and the delayed ($1.4 < t_{Trig} < 4.4 \mu\text{s}$) time windows.

For the likelihood fit, cuts were loosened, increasing the sensitivity to a CEvNS signal, to 0–300 keVee, 0.4–4.4 μs relative to the SNS timing signal, and from F_{prompt} values ranging from 0.55–0.95. The lack of CEvNS events with reconstructed energy $E_{reco} > 50$ keVee and the lack

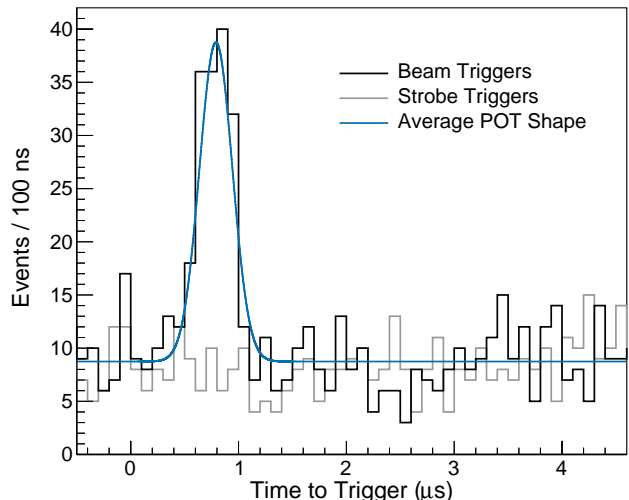


FIG. 6. Time distribution of beam-on and strobe samples in the BRN-enhanced energy window. The blue curve is that expected from the timing shape of the SNS POT signal scaled to the beam-on-target excess.

of BRN events in the delayed window ($t_{Trig} > 1.4 \mu\text{s}$) serves to separate the BRN and CEvNS signals. The efficiencies as a function of nuclear recoil energy for these cuts is seen in Fig. 5.

Systematic errors were assigned to the beam-related (CEvNS and BRN) predictions for the quenching factor and pulse-finding threshold. These uncertainties were dominated by the uncertainty of the NR PSD band in the CEvNS energy region due to the high threshold of the ^{252}Cf calibration datasets. An additional source of uncertainty was included on the overall BRN normalization due to the extrapolation of the BRN rate from the minimal-shielded dataset. For the cuts-based analysis, correlated systematic errors were calculated and a goodness-of-fit (χ^2) quantity was determined for the beam excess compared to the MC prediction. For the cross section limits from the likelihood fits, alternative PDFs incorporating $\pm 1\sigma$ excursions for each systematic were fit to the data, and the difference from the central value result were added in quadrature as a measure of the systematic uncertainty.

RESULTS

The resulting sample from the BRN-enhanced cuts-based analysis (0–700 keVee) over the full time range is shown in Fig. 6. Note the clear evidence of BRNs with time structure consistent with the POT trace from the SNS beam. Note also that there is no evidence of this signal in the delayed ($t_{Trig} > 1.4 \mu\text{s}$) region. This is consistent with the hypothesis that the BRN that reach the CENNS-10 detector inside of the shielding are the result

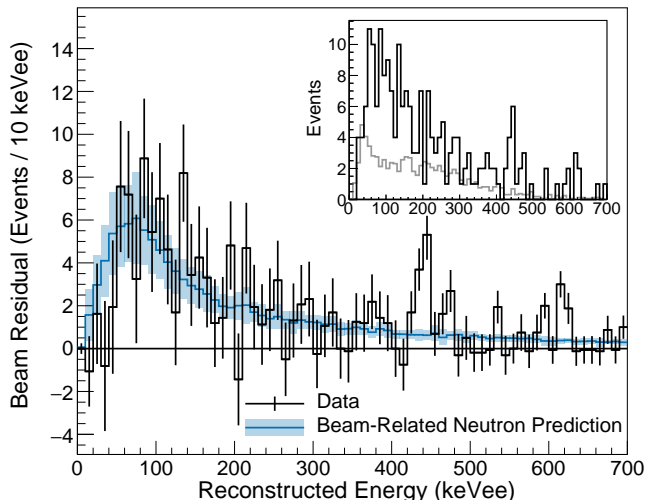


FIG. 7. Energy distribution of the cuts-based analysis beam-residual event sample in the prompt time window along with the BRN prediction. The error bars are statistical and the error band on the prediction is systematic. Plot inlay shows un-subtracted spectra from the prompt beam-on triggers (black) and the expected beam-unrelated background as measured with strobe triggers (gray).

of fast neutrons in Neutrino Alley that lose sufficient energy to create low-energy nuclear recoils in LAr. This is verified by MC simulations.

The reconstructed energy distribution from this sample in the prompt time region ($0.4 < t_{Trig} < 1.4 \mu\text{s}$) is shown in Fig. 7. The beam-related excess of $126 \pm 15(\text{stat.})$ events in this sample is consistent with the BRN prediction of $112 \pm 30(\text{syst.})$ events. The uncertainty on the BRN prediction is dominated by the uncertainty in the overall fast neutron flux ($\pm 20\%$), the uncertainty of the NR PSD band mean near threshold ($\pm 19\%$), the pulse-finding threshold ($\pm 5\%$), and the quenching factor ($\pm 4\%$). The predicted CEvNS signal in this sample is < 1 detected event. A comparison of the data with the predicted BRN energy spectrum gives a χ^2/N_{bins} , including correlated uncertainties, of $99/70$ ($2.0/3$ in the CEvNS energy ROI). The excess of events above prediction at $E \approx 440$ keVee has a global p-value under the null hypothesis of 1.7% and is above the energy region of interest for the likelihood fit.

The energy distribution of events in the delayed sample is shown in Fig. 8. In the CEvNS energy region 0–30 keVee, an excess of $1 \pm 4(\text{stat.})$ events is observed, with a predicted CEvNS sample of < 1 event with an uncertainty dominated by the pulse-finding threshold ($\pm 35\%$), the NR PSD band mean behavior near threshold ($\pm 30\%$), the quenching factor ($\pm 15\%$), and the uncertainty in the neutrino flux ($\pm 10\%$). The first two errors are large because the CEvNS events are so near the threshold in this dataset. In addition, there are

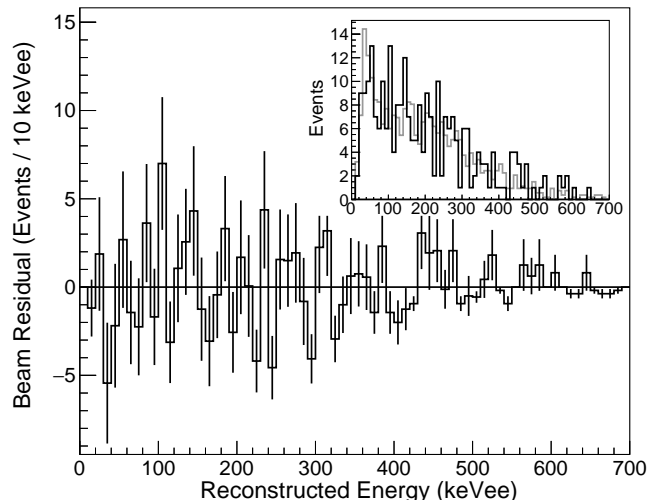


FIG. 8. Energy distribution of the cuts-based analysis beam-residual event sample in the delayed time window. Plot inlay shows un-subtracted beam-on spectrum (black) along with the expected beam-unrelated backgrounds as measured with strobe triggers (gray).

TABLE I. Results of a maximum likelihood fit to the data (details in text). The quoted beam-unrelated background counts includes the statistical uncertainty in its determination from the strobe trigger sample.

sample size	4663
beam-unrelated background	4700 ± 34
fit BRN	$126 \pm 18(\text{stat.}) \pm 28(\text{syst.})$
1σ (68% C.L.) CEvNS events	< 7.4
1σ cross section	$< 3.4 \times 10^{-39} \text{ cm}^2$
1σ cross section sensitivity	$< 7.1 \times 10^{-39} \text{ cm}^2$

$9 \pm 18(\text{stat.})$ events in the extended energy range out to 700 keVee, consistent with earlier measurements [18, 44] indicating no delayed beam-related neutron flux in Neutrino Alley.

The likelihood fit was performed by passing a total of 4663 events surviving the likelihood cuts to a 3D likelihood function in energy, time, and F_{prompt} space including beam-unrelated and BRN backgrounds along with a CEvNS signal. A profile likelihood curve was calculated as a function of the number of CEvNS events and a frequentist confidence limit (C.L.) method [45–47], along with a simple treatment of the large systematic errors, was used to place an upper limit on the number of CEvNS events of < 7.4 events. This result can be used to place a 68% C.L. on the stopped-pion flux-averaged cross section of $< 3.4 \times 10^{-39} \text{ cm}^2$, within twice the Standard Model prediction of $1.8 \times 10^{-39} \text{ cm}^2$ [48]. These results are summarized in Table I and the projections in time, F_{prompt} , and reconstructed energy can be seen in Fig. 9.

Using the same frequentist method a 90% C.L. on the

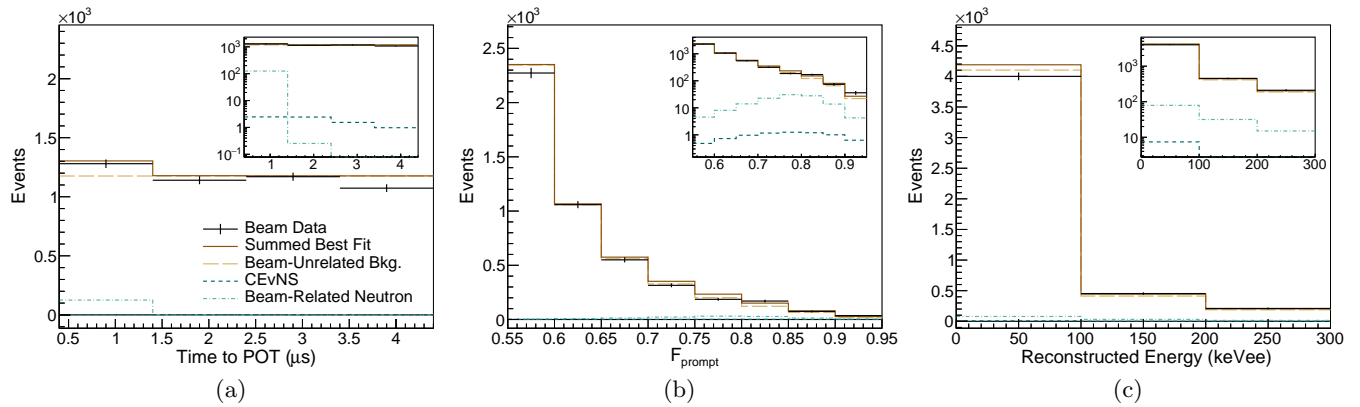


FIG. 9. Projections of likelihood best-fit solutions together with the data in (a) time, (b) F_{prompt} , and (c) reconstructed energy. The CEvNS curve shown is from the 68% confidence limit found. Inlaid plots show the spectra in log-scale to make the small contributions from the predicted CEvNS distribution more visible.

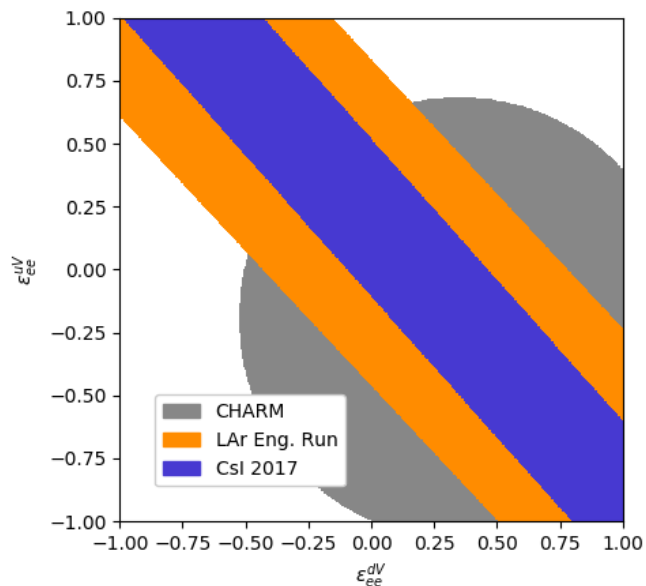


FIG. 10. 90% CL on NSI parameters ϵ_{ee}^{uV} and ϵ_{ee}^{dV} from this CENNS-10 engineering run. The earlier CsI[Na] result [18] is confirmed and much of the pre-COHERENT phase space allowed by CHARM [49] is ruled out.

cross section of $<8.3 \times 10^{-39} \text{ cm}^2$ was extracted and used to set limits on the NSI couplings $\epsilon_{ee}^{uV}, \epsilon_{ee}^{dV}$ [9]. Under the assumption of heavy mediators, these couplings result in an overall scaling factor to the CEvNS cross section [18]. Fig. 10 indicates the allowed parameter values consistent with this 90% C.L. cross section.

CONCLUSIONS

In this first result from the CENNS-10 liquid argon detector as part of the COHERENT experiment, a dataset taken as part of an engineering run corresponding to

4.2×10^{22} protons on the SNS target collected from Feb. 24, 2017 to May 28, 2017, has been analyzed. The energy threshold in this configuration is not adequate for high sensitivity to CEvNS. However, beam-related neutrons were characterized, further refining constraints on this important background which will inform future measurements. In addition, no BRN were observed in the delayed time window, outside of the beam pulse, consistent with previous measurements. The observation of no significant beam excess does allow for a first limit on the CEvNS cross section on argon within twice the SM prediction and for a corresponding limit on NSI.

The CENNS-10 detector was upgraded in the summer of 2017 to improve light collection and lower the energy threshold to 20 keVnr, and additional shielding was installed to minimize the dominant beam-unrelated background in Neutrino Alley. CENNS-10 has collected >6 GWhr of data in this configuration with the sensitivity to make a first observation of CEvNS on argon. COHERENT is also working towards CEvNS measurements with a 2t NaI array, also sensitive to charged current interactions, as well as with 16 kg p-type point-contact Ge to maximize the neutrino physics capabilities at the SNS [48].

ACKNOWLEDGMENTS

The COHERENT collaboration acknowledges the generous resources provided by the ORNL Spallation Neutron Source and thanks Fermilab for the continuing loan of the CENNS-10 detector. We also acknowledge support from: the Alfred P. Sloan Foundation, the Consortium for Nonproliferation Enabling Capabilities, the Institute for Basic Science (Korea, grant No. IBS-R017-G1-2019-a00), the National Science Foundation, the Russian Foundation for Basic Research (proj.# 17-02-01077 A), and the U.S. Department of Energy Office of Sci-

ence. Laboratory Directed Research and Development funds from ORNL and LLNL also supported this project. This research used the Oak Ridge Leadership Computing Facility, which is a DOE Office of Science User Facility.

-
- [1] D. Z. Freedman, Phys. Rev. **D9**, 1389 (1974).
- [2] V. B. Kopeliovich and L. L. Frankfurt, JETP Lett. **19**, 145 (1974), [Pisma Zh. Eksp. Teor. Fiz.19,236(1974)].
- [3] P. S. Amanik and G. C. McLaughlin, Journal of Physics G: Nuclear and Particle Physics **36**, 015105 (2009).
- [4] M. Cadeddu *et al.*, Phys. Rev. Lett. **120**, 072501 (2018).
- [5] M. Cadeddu and F. Dordei, Phys. Rev. D **99**, 033010 (2019).
- [6] K. Patton, J. Engel, G. C. McLaughlin, and N. Schunck, Phys. Rev. **C86**, 024612 (2012), arXiv:1207.0693 [nucl-th].
- [7] D. Aristizabal Sierra, J. Liao, and D. Marfatia, JHEP **06**, 141 (2019), arXiv:1902.07398 [hep-ph].
- [8] M. Hoferichter, P. Klos, J. Menndez, and A. Schwenk, Phys. Rev. **D99**, 055031 (2019), arXiv:1812.05617 [hep-ph].
- [9] J. Barranco *et al.*, Journal of High Energy Physics **2005**, 021 (2005).
- [10] K. Scholberg, Phys. Rev. D **73**, 033005 (2006).
- [11] J. Barranco *et al.*, Phys. Rev. D **76**, 073008 (2007).
- [12] B. Dutta *et al.*, Phys. Rev. D **93**, 013015 (2016).
- [13] D. K. Papoulias and T. S. Kosmas, Phys. Rev. D **97**, 033003 (2018).
- [14] L. M. Krauss, Physics Letters B **269**, 407 (1991).
- [15] P. Coloma and T. Schwetz, Phys. Rev. D **94**, 055005 (2016).
- [16] P. Coloma *et al.*, Journal of High Energy Physics **2017**, 116 (2017).
- [17] P. Coloma *et al.*, Phys. Rev. D **96**, 115007 (2017).
- [18] D. Akimov *et al.* (COHERENT), Science **357**, 1123 (2017), arXiv:1708.01294 [nucl-ex].
- [19] R. Tayloe (COHERENT), *Proceedings, Light Detection in Noble Elements (LIDINE 2017): Menlo Park, CA, USA, September 22-24, 2017*, JINST **13**, C04005 (2018), arXiv:1801.00086 [physics.ins-det].
- [20] S. J. Brice *et al.*, Phys. Rev. D **89**, 072004 (2014).
- [21] V. M. Gehman *et al.*, Nucl. Instrum. Meth. **A654**, 116 (2011), arXiv:1104.3259 [astro-ph.IM].
- [22] C. Benson *et al.*, The European Physical Journal C **78**, 329 (2018).
- [23] D. N. McKinsey *et al.*, Nuclear Instruments and Methods in Physics Research Section B: Beam Interactions with Materials and Atoms **132**, 351 (1997).
- [24] P. Agnes *et al.*, Physics Letters B **743**, 456 (2015).
- [25] P. Agnes *et al.* (DarkSide Collaboration), Phys. Rev. **D98**, 102006 (2018).
- [26] R. Aja *et al.* (DEAP), (2019), arXiv:1902.04048 [astro-ph.CO].
- [27] C. Adams *et al.* (The MicroBooNE Collaboration 1), Phys. Rev. D **99**, 091102 (2019).
- [28] T. Doke *et al.*, Nucl. Instrum. Meth. **A291**, 617 (1990).
- [29] D. Gastler *et al.*, Phys. Rev. C **85**, 065811 (2012).
- [30] H. Cao *et al.* (SCENE Collaboration), Phys. Rev. D **91**, 092007 (2015).
- [31] W. Creus *et al.*, Journal of Instrumentation **10**, P08002 (2015).
- [32] P. Agnes *et al.* (The ARIS Collaboration), Phys. Rev. D **97**, 112005 (2018).
- [33] A. Hitachi *et al.*, Phys. Rev. B **27**, 5279 (1983).
- [34] P.-A. Amaudruz *et al.*, Astroparticle Physics **85**, 1 (2016).
- [35] P. Benetti *et al.*, Astroparticle Physics **28**, 495 (2008).
- [36] W. H. Lippincott *et al.*, Phys. Rev. C **78**, 035801 (2008).
- [37] H. Back *et al.*, Physics Procedia **37**, 1105 (2012), proceedings of the 2nd International Conference on Technology and Instrumentation in Particle Physics (TIPP 2011).
- [38] H. O. Back *et al.*, (2012), arXiv:1206.6024 [astro-ph.IM], arXiv:1204.6024 [astro-ph.IM].
- [39] P. Agnes *et al.* (DarkSide Collaboration), Phys. Rev. D **93**, 081101 (2016).
- [40] R. Cooper, L. Garrison, H. O. Meyer, T. Mikev, L. Rebenitsch, and R. Tayloe, in *Particles and fields. Proceedings, Meeting of the Division of the American Physical Society, DPF 2011, Providence, USA, August 9-13, 2011* (2011) arXiv:1110.4432 [hep-ex].
- [41] M. R. Heath, *A First Search for Coherent Elastic Neutrino-Nucleus Scattering with Liquid Argon*, Ph.D. thesis, Indiana U., Bloomington (main) (2019), 10.5967/jmrj-9078.
- [42] R. Acciarri *et al.*, JINST **5**, P06003 (2010).
- [43] S. Agostinelli *et al.* (GEANT4), Nucl. Instrum. Meth. **A506**, 250 (2003).
- [44] D. Akimov *et al.* (COHERENT), (2015), arXiv:1509.08702 [physics.ins-det].
- [45] G. J. Feldman and R. D. Cousins, Phys. Rev. **D57**, 3873 (1998), arXiv:physics/9711021 [physics.data-an].
- [46] R. T. Thornton, *Search for Light Dark Matter Produced in a Proton Beam Dump*, Ph.D. thesis, Indiana U. (2017).
- [47] A. A. Aguilar-Arevalo *et al.* (MiniBooNE-DM Collaboration), Phys. Rev. Lett. **118**, 221803 (2017).
- [48] D. Akimov *et al.* (COHERENT), (2018), arXiv:1803.09183 [physics.ins-det].
- [49] J. Dorenbosch *et al.* (CHARM), Phys. Lett. **B180**, 303 (1986).